Journal of Engineering Science and Technology
Vol. 6, No. 5 (2011) 558 - 574

EFFECT OF FORCED ROTATING VANELESS DIFFUSERS ON CENTRIFUGAL COMPRESSOR STAGE PERFORMANCE

M. GOVARDHAN*, S. SERALATHAN

Department of Mechanical Engineering
Indian Institute of Technology Madras, Chennai 600 036, India
*Corresponding Author: gova@iitm.ac.in

Abstract

Non-uniform flow at the exit of the centrifugal impeller mixes in the vaneless space of the diffuser causing a rise in static pressure as well as significant loss of total pressure. These mixing losses are usually an important source of inefficiency. Forced rotating vaneless diffusers is one such concept which reduces the energy losses associated with diffusion. Forced rotating vaneless diffuser involves the concept of blade cutback and shroud extension. In the present computational investigations, the effects of blade cutback of 5%, 10% and 20% of vane length, shroud extension of 10%, 20%, 30% and 40% of impeller tip diameter and impeller without shroud extension on flow diffusion and performance are analyzed, while all the other dimensions remaining same. The performance characteristics of various blade cutback configurations are less in terms of efficiency, energy coefficient as well as static pressure rise. The objective of obtaining higher static pressure rise with wide operating range and reduced losses over stationary vaned diffuser is achieved by shroud extension of 30%, followed by shroud extension of 20%.

Keywords: Diffuser, Blade, Centrifugal compressor, Efficiency, Shroud extension.

1. Introduction

Non-uniform flow at the exit of the centrifugal impeller mixes in the vaneless space of the diffuser causing a rise in static pressure as well as significant loss of total pressure. These mixing losses are usually an important source of inefficiency. Centrifugal impeller flows investigated by number of researchers have confirmed the existence of separated zones at the exit of the impeller, which limit the impeller diffusion. Therefore, it is necessary to develop methods which reduce the energy losses associated with diffusion and also increase the stable

Nomenclatures

B	Blade width, m
C	Absolute velocity, m/s
C_m	Meridional velocity, m/s
C_p	Static pressure coefficient
C_{po}	Total pressure coefficient
C_u	Tangential velocity, m/s
D	Diameter, m
N	Rotational speed, rev./min
P	Static pressure, N/m^2
P_o	Total pressure, N/m^2
R	Radius ratio = r/r_2
W	Specific work, m^2/s^2
U	Impeller tip speed or Peripheral velocity, m/s
V	Volume flow rate, m^3/s
X	Span normalized; non-dimensional axial distance = x/b
x	Axial distance, m

Greek Symbols

α	Flow angle, deg.
β	Blade angle, deg.
ρ	Density of air, kg/m^3
Φ	Flow coefficient = C_m / U_2
η	Efficiency
ψ	Energy coefficient = $2W/ U_2^2$
ψ_{Loss}	Stagnation pressure loss coefficient = $2(P_{02}-P_0) / \rho U_2^2$
ψ_p	Static pressure recovery coefficient = $2(P-P_2) / \rho U_2^2$

Subscripts

A	Front shroud
B	Back shroud
h	Hub
m	Meridional
o	Total
s	Static
u	Tangential
1	Impeller inlet
2	Impeller exit
2_{BLADE}	Impeller blade exit
2_{DISKS}	Impeller disks exit
2_{BLADE}	Impeller blade exit after blade cutback
3	Stationary vaneless diffuser inlet
4	Stationary vaneless diffuser exit

Subscripts

=	Mass averaged value

Abbreviations

BC	Blade cutback
BC 05	Corresponds to blade cutback by 5% with respect to its vane length to form a forced rotating vaneless diffuser
BC 10	Corresponds to blade cutback by 10% with respect to its vane length to form a forced rotating vaneless diffuser
BC 20	Corresponds to blade cutback by 20% with respect to its vane length to form a forced rotating vaneless diffuser
RVD	Rotating vaneless diffuser
SE	Shroud extension
SE 20	Corresponds to shroud extension with diameter ratio 1.2 with exit of the impeller to form a forced rotating vaneless diffuser
SE 30	Corresponds to shroud extension with diameter ratio 1.3 with exit of the impeller to form a forced rotating vaneless diffuser
SE 40	Corresponds to shroud extension with diameter ratio 1.4 with exit of the impeller to form a forced rotating vaneless diffuser
SE10	Corresponds to shroud extension with diameter ratio 1.1 with exit of the impeller to form a forced rotating vaneless diffuser
SVD	SVD corresponds to Stationary Vaneless Diffuser with diffuser diameter ratio 1.4 with exit of the impeller

operating ranges of diffusion systems. Rotating vaneless diffusers is one such concept studied and tried out by the researchers.

Rotating vaneless diffusers are of two types: Free rotating vaneless diffuser and forced rotating vaneless diffuser. Free rotating diffusers are separate entity and rotate at a fraction of the impeller speed by using a suitable arrangement, whereas, forced rotating diffusers are integral with the impeller and rotate at the same speed as the impeller.

In free rotating vaneless diffuser, the walls of the vaneless region were rotated independently of the impeller [1]. The diffuser speed becomes a fraction of the impeller speed so that the shear forces between the flow and diffuser wall are greatly reduced. Thus, the boundary layer growth within the rotating diffuser is smaller than in the corresponding stationary diffuser, and the compressor performance improves both from frictional and flow profile considerations. Still, another attempt at obtaining the advantages of a rotating diffuser was made in [2], where the rotating diffuser section was an extension of the rotor shroud. Sapiro [3] conducted experimental investigations and found that impeller-extended shrouds for purpose of improving the efficiency of the stage, will only benefit to a small extent high specific speed stages and detrimental to low specific speed stages.

Another way of achieving the rotating diffuser is by blade cutback, which involves blade trimming. In this arrangement shroud and hub disk are not machined. This is an appropriate means of reducing the polytropic head of an impeller [4, 5]. The authors reported the advantages of rotating diffuser with small cutback rate in achieving additional static pressure recovery.

The designer should pay attention to the fact that flow through the diffuser takes place against the positive pressure gradient and there is a possibility for the flow to separate from wall of the diffuser or from the wall of the vane suction surface in case of vane diffuser. Diffuser is followed by volute, where further deceleration of fluid takes place. However, limited information is available in open literature about rotating diffuser design and performance, although the subject has been discussed in [1, 6, 7].

The objective of the present investigations is to study computationally the effects of blade cutback, shroud extension on the flow diffusion and performance characteristics of a centrifugal blower. The impeller with blade cutback of 5%, 10% and 20% of vane length, impeller with shroud extension of 10%, 20%, 30% and 40% of impeller tip diameter and impeller without shroud extension are analyzed, while all the other dimensions remaining same.

2. Computational Model and Numerical Formulation

2.1. Governing equations

The governing equations are integrated over each control volume, such that the relevant quantity (mass, momentum, energy, etc.) is conserved in a discrete sense for each control volume.

- **Continuity equation**

$$\frac{\partial \rho}{\partial t} + \nabla \bullet (\rho C) = 0 \tag{1}$$

where $C = u\hat{i} + v\hat{j} + w\hat{k}$

As the flow is assumed steady, $\frac{\partial \rho}{\partial t} = 0$ and continuity equation then reduces to

$$\nabla \bullet (\rho C) = 0 \tag{2}$$

- **Momentum equation**

$$\frac{\partial \rho C}{\partial t} + \nabla \bullet (\rho C \otimes C) = \nabla \bullet \left(-\rho\delta + \mu\left(\nabla C + (\nabla C)^T\right)\right) + S_M \tag{3}$$

where S_M refers to momentum sources.

As the flow is assumed to be in steady state, $\frac{\partial \rho C}{\partial t} = 0$ and momentum equation then reduces to

$$\nabla \bullet (\rho C \otimes C) = \nabla \bullet \left(-\rho\delta + \mu\left(\nabla C + (\nabla C)^T\right)\right) + S_M \tag{4}$$

- **Energy equation**

$$\frac{\partial \rho h_o}{\partial t} - \frac{\partial p}{\partial t} + \nabla \bullet (\rho C h_o) = \nabla \bullet (\lambda \nabla T) + S_E \tag{5}$$

For a steady flow, $\frac{\partial \rho h_o}{\partial t} = 0$ and $\frac{\partial p}{\partial t} = 0$, and the energy equation in this case reduces to

$$\nabla \bullet \left(\rho C h_o\right) = \nabla \bullet \left(\lambda \nabla T\right) + S_E \tag{6}$$

where $h = h(p, T)$ and h_o is the specific total enthalpy

$$h_o = h + \frac{1}{2} C^2 \tag{7}$$

If viscous work is significant, an additional term is used in the RHS of the energy equation to account for the effect of viscous shear. The energy equation then becomes,

$$\frac{\partial \rho h_o}{\partial t} - \frac{\partial p}{\partial t} + \nabla \cdot \left(\rho C h_o\right) = \nabla \cdot \left(\lambda \nabla T\right) + \left[\nabla \cdot \left\{\mu \left[\nabla C + \left(\nabla C\right)^T - \frac{2}{3} \nabla \cdot C\delta\right] C\right\} + S_E\right] \tag{8}$$

The additional term represents the work due to external momentum sources.

A total of seven unknowns are involved, u, v, w, p, T, h, p, in five equations but the set can be closed by adding two algebraic thermodynamic equations, namely; equation of state relating density, ρ, to temperature, T, and pressure, p, and constitutive equation relating enthalpy, h, to temperature, T, and pressure, p.

- **Equation of state for ρ**

For an ideal gases, the relationship described by ideal gas law,

$$\rho = \frac{w\left(p + p_{ref}\right)}{R_o T} \tag{9}$$

where w is the molecular weight of the gas, and R_o is the universal gas constant.

- **Equation of state for enthalpy (constitutive equation)**

The algebraic thermodynamic relation for enthalpy is:

$$h_2 - h_1 = \int_{T_1}^{T_2} C_p dT + \int_{p_1}^{p_2} \frac{1}{\rho}\left[1 + \frac{T}{\rho}\left(\frac{\partial \rho}{\partial T}\right)_p\right] dp \tag{10}$$

In the above equation, the first part is equivalent to the change in enthalpy for an ideal gas and the second step is a correction required for the real fluid. If both density and specific heat are constants, the above equation then reduces to

$$dh = C_p dT + \frac{dp}{\rho} \tag{11}$$

For an ideal gases, the relationship described by ideal gas law.

- **Rotational forces**

For flows with rotating frame of reference, rotating at a constant angular velocity ω, additional sources of momentum are required to account for the effect of Coriolis force and the centrifugal force.

$$SM_{rot} = S_{cor} + S_{cfg} \tag{12}$$

$S_{cor} = -2\rho\omega \times C_{rot}$ and $S_{cfg} = -\rho\omega \times (\omega \times r)$

where r is the location vector and C_{rot} is the relative frame velocity (i.e., the rotating frame velocity for a rotating frame of reference).

2.2. Modelling

For geometry creation and mesh generation ICEM CFD 10 is used in the present investigation. The impeller chosen for the present investigations was manufactured in the laboratory and tested. The experimental data is also available. Hence, it was decided to model the impeller with same dimensions and conduct CFD investigations. The geometric details of the impeller and various forms of rotating vaneless diffusers used in the present investigations are given in the Table 1 to Table 3. All the angles are with respect to the tangential direction. The centrifugal impeller used in the present investigations is a radial outflow impeller with 18 blades of uniform thickness. The impeller considered is a shrouded impeller on both sides. The blade angle at exit is set to 90^0 with radial outlet flow. The hub is attached to the impeller [back shroud] and rotates along with the impeller. The present computational analysis approach consists of two domains viz., impeller and diffuser, which are modeled and meshed together as a single domain.

Table 1. Geometric Dimensional Details: Impeller and Stationary Vaneless Diffuser.

Impeller		
Diameter at inlet of the impeller	D_1	215.2 mm
Diameter at exit of the impeller (Disks)	$D_{2\ DISKS}$	570 mm
Diameter at exit of the impeller (Blade)	$D_{2\ BLADE}$	570 mm
Number of blades	Z	18
Width of the blade at exit	b_2	27.6 mm
Width of blade at inlet	b_1	58.5 mm
Blade angle at the inlet	β_1	44.6^o
Blade angle at the exit	β_2	90^o
Diameter of the hub	D_h	100 mm
Rotational speed of the impeller	N	1500 rpm
Stationary Vaneless Diffuser [SVD]		
Diffuser Diameter ratio	D_4/D_3	1.40
Diffuser Outlet Diameter	D_4	798 mm
Diffuser Inlet Diameter	D_3	570 mm

Table 2. Geometric Dimensional Details: Impeller with Extended Shrouds and Stationary Vaneless Diffuser.

	Impeller with10% extended shroud with respect to D_2 [SE 10]	Impeller with 20% extended shroud with respect to D_2 [SE 20]	Impeller with 30% extended shroud with respect to D_2 [SE 30]	Impeller with 40% extended shroud with respect to D_2 [SE 40]
$D_{2\ BLADE}$	570 mm	570 mm	570 mm	570 mm
$D_{2\ DISKS}$	627 mm	684 mm	741 mm	798 mm
D_3	627 mm	684 mm	741 mm	---
D_4	798 mm	798 mm	798 mm	---

Table 3. Geometric Dimensional Details: Impeller Involving Blade Cutback and Stationary Vaneless Diffuser.

	Impeller with 5% blade cutback with respect to vane length [BC 05]	Impeller with 10% blade cutback with respect to vane length [BC 10]	Impeller with 20% blade cutback with respect to vane length [BC 20]
$D_{2\ DISKS}$	570 mm	570 mm	570 mm
$D_{2\ BLADE}$	552.26 mm	534.52 mm	499.04 mm
D_3	570 mm	570 mm	570 mm
D_4	798 mm	798 mm	798 mm

Other dimensional details of the impeller remaining the same as mentioned in Table 1

Preference was given to rectangular co-ordinate frame, as various dimensions were available only in this co-ordinate frame. The tolerance of geometry creation is set as 0.001 mm. Flow is treated as periodic, so that instead of modeling the entire 360^0 geometry of the impeller and diffuser, one blade passage (single passage approach) is modeled and solved. The passage considered is half the blade spacing on either side of the blade.

The modeling of the blade profiles was done such that the curves are smooth and continuous. Apart from the blade surfaces, other surfaces enclosing the domain are inlet, outlet, periodic pairs, hub surface and shroud surface. Inlet and outlet surfaces were developed normal to the axis. These above surfaces constitute the bounding surfaces of the domain and a fluid domain was developed from these bounding surfaces.

2.3. Grid generation

Unstructured grid is generated using tetrahedral elements with flat prism shaped cells in the near wall zones to obtain a finer resolution in the boundary layer. Grid independence studies were carried out to validate the numerical data with the experimental results. Table 4 gives the details of the final grid size for various configurations.

The reference pressure is set to 101325 Pa. The fluid is set as air at 25°C. The density and dynamic viscosity at this temperature is fixed. Fluid is kept as non-

buoyant. The fluid is considered as incompressible and sub-sonic. Domain motion was set as rotating. The axis of rotation along with the speed of rotation is specified. Simulation type was set as steady state. Figure 1 shows the computational domain with boundary conditions.

Table 4. Details of the Grid for Various Rotating Vaneless Diffusers Used in the Present Investigation.

Forced Rotating Vaneless Diffuser Concepts		
Computational Domain	No. of Nodes	No. of Elements
SVD	240442	899831
Shroud extend 10%	242052	902109
Shroud extend 20%	241435	903135
Shroud extend 30%	218934	855481
Shroud extend 40%	240442	899831
Blade cutback 5%	190970	790298
Blade cutback 10%	237199	886879
Blade cutback 20%	243936	910605

2.4. Turbulence modeling

A good modeling of turbulence is necessary for obtaining a better prediction on flow separation. Standard k-ω and k-ω based Shear Stress Transport (SST) turbulence models were used and the results were compared with the experimental. As numerical values from k-ω model are closer to the experimental values [4], further investigations were carried out with this turbulence model.

2.5. Boundary conditions

A specific flow prediction will correspond to a specific set of boundary conditions. Total pressure with boundary layer profile is used for inlet boundary condition. Mass flow rate is given at outlet. The mass flow rate is calculated from the chosen flow coefficient. Thus, with total pressure specification at the inlet and the mass flow rate at the outlet, velocity and pressure distribution within the domain can be computed.

As passage, with half the pitch on either side of the blade is being solved; the planes on either side of the blade will make periodic pair of surfaces. Periodic boundary conditions are given on the sides of the domain. Rotational periodicity was enforced about the axis of rotation.

The blades, hub, shroud and rotating diffuser walls are given wall boundary condition rotating with angular velocity equal to that of domain. Hence, they are stationary with respect to relative frame of reference. No-slip conditions were enforced on the walls and wall roughness was neglected by assuming it as a smooth wall. Numerical investigations are carried out using commercial CFD

code, namely CFX 11.0. A convergence criterion of 1×10^{-4} is defined for the present computation.

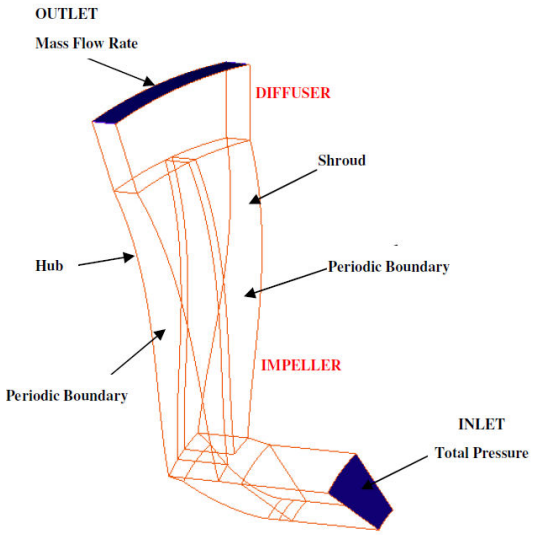

Fig. 1. Computational Domain of a Single Passage Modeled for Centrifugal Impeller and Vaneless Diffuser showing the Boundary Conditions.

3. Results and Discussion

The results from the CFD study are validated with the measured static pressure distribution across the width at the exit of the radial bladed impeller as reported in [4]. As shown in Fig. 2, both computational and experimental values are in good agreement.

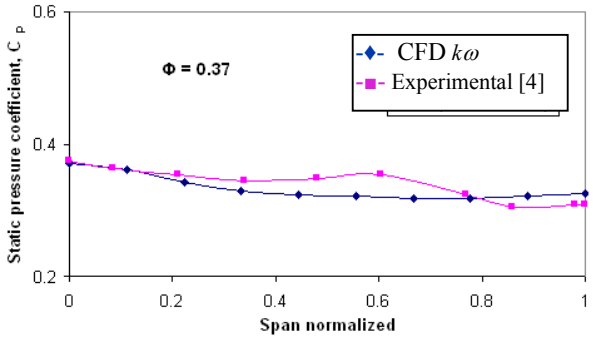

Fig. 2. Comparison of Non-Dimensional Static Pressure Distribution Measured across the Width at the Exit of the Radial Tipped Impeller alone [Φ = 0.37, N= 1500 rpm].

3.1. Performance characteristics

The performance characteristics of various blade cutback and shroud extension configurations are shown in Figs. 3 and 4 as against flow coefficient, ϕ. Flow coefficient is defined as the ratio of meridional velocity, c_m, and peripheral velocity at outlet, U_2. Flow coefficient is proportional to the volume flow rate through the machine. SE 10 has the highest efficiency followed by SE 20 and SE 30. The values are above stationary vaned diffuser whereas blade cutback configurations exhibit efficiency lower than SVD. As expected, efficiency decreases with flow coefficients for all configurations. Energy coefficient, ψ, for all shroud extension configurations is higher than SVD whereas for blade cutback it is lower (Fig. 4). Energy coefficient, ψ, is defined as $(2W/ U_2^2)$, where W is specific work. SE 40 and SE 30 produce highest and lowest energy coefficient at all flow rates.

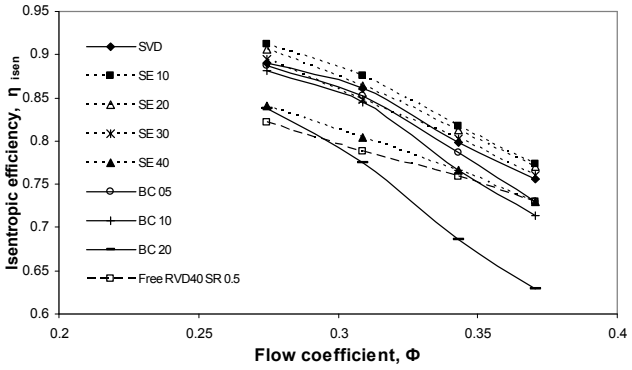

Fig. 3. Performance Characteristics Curves for SVD, Shroud Extension and Blade Cutback Concepts - Variation of Isentropic Efficiency.

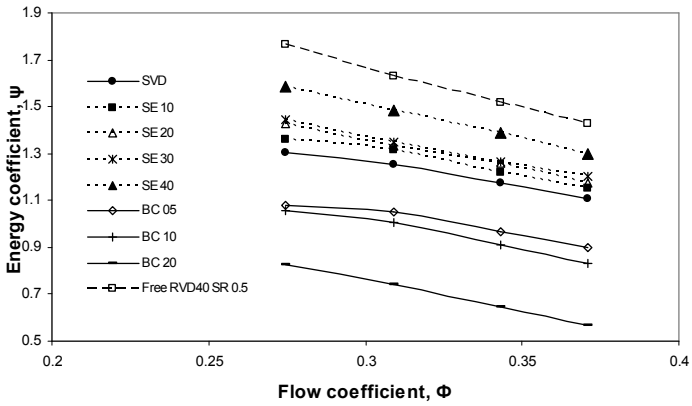

Fig. 4. Performance Characteristics Curves for SVD, Shroud Extension and Blade Cutback concepts - Variation of Energy Coefficient.

3.2. Mass averaged stagnation pressure loss coefficient

Mass averaged stagnation pressure loss coefficient (ψ_{loss}) against radius ratio is shown in Fig. 5. ψ_{loss} is defined as 2 (P_{02} - P_0)/ρU_2^2, where P_{02} and P_0 are mass averaged stagnation pressures at impeller and diffuser exit respectively. The mass averaged stagnation pressure loss coefficient increases with radius ratio for all configurations except for SE 40. Increase in stagnation pressure loss coefficient indicates the amount of losses (mixing and friction) occurred in the flow passage. BC 05 has maximum rise in the stagnation pressure loss coefficient compared to the SVD. The SE 40 shows a gain in total pressure after R = 1.25, due to energy added by rotating extended shrouds in overcoming losses due to friction. For other configurations, the stagnation pressure loss coefficient is less than that of the SVD.

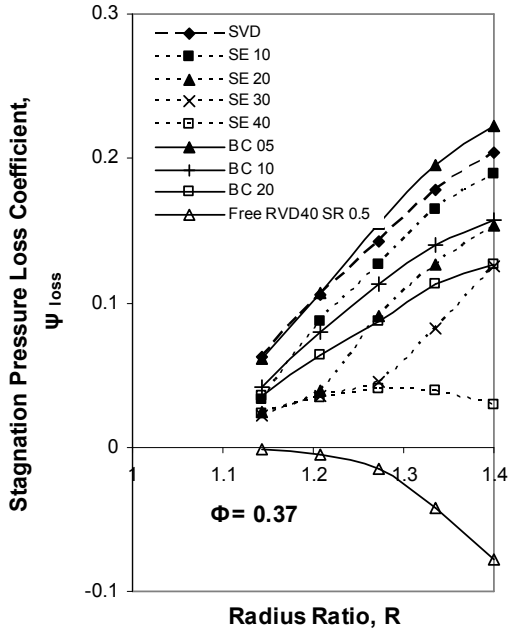

Fig. 5. Radial Distribution of Mass Averaged Stagnation Pressure Loss Coefficient for SVD, Shroud Extension and Blade Cutback.

If the vaneless diffuser sidewalls are stationary, the dynamic head and the logarithmic path length of the flow causing the shear losses are functions of the magnitude and direction of the absolute velocity leaving the impeller. On the other hand, if the vaneless diffuser sidewalls are rotating, the dynamic head and the path length of the flow causing the shear losses are a function of the magnitude and direction of the relative velocity in the diffuser, which is much smaller and more radial than the absolute velocity. With the result, frictional losses in rotating vaneless diffuser will be smaller than stationary vaneless diffuser. The same is reflected for blade cutback and shroud extension diffusers, which have higher flow angles than SVD at impeller outlet.

3.3. Mass averaged static pressure recovery coefficient (ψ_p)

Mass averaged static pressure recovery coefficient against radius ratio is shown in Fig. 6. Static pressure recovery coefficient, ψ_p is defined as $2(P - P_2)/\rho U_2^2$, where P_2 and P are mass averaged static pressures at impeller exit and diffuser exit respectively. Blade cutback exhibits less static pressure recovery compared to SVD, whereas, shroud extension offers higher static pressure recovery than SVD. The static pressure recovery is approximately same for all shroud extension configurations up to radius ratio, R = 1.14, thereafter the static pressure rise is higher in SE 40, followed by SE 30, SE 20 and SE 10 respectively which is reflected in the higher static pressure recovery at the exit of the diffusers. This explains that the rate of diffusion is higher in shroud extension configurations compared to SVD.

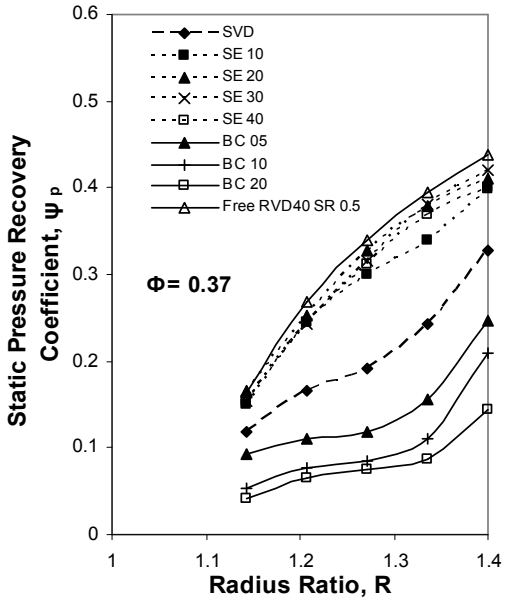

Fig. 6. Radial Distribution of Mass Averaged Static Pressure Recovery Coefficient for SVD, Shroud Extension and Blade Cutback.

The static pressure recovery in blade cutback shows a gradual increase up to 3/4th of the stationary vaneless passage and thereafter static pressure recovery occurs rapidly till the exit of the diffuser. However, the values are still less than SVD for all flow coefficients. This may be due to alteration in blade tip geometry made by blade cutback which has an effect on the velocities of the through flow. BC 20 offers a poor static pressure recovery for all the cases irrespective of flow rates.

3.4. Mass averaged absolute velocity

Mass averaged absolute velocity is shown in Fig. 7. As the radius increases, velocity decreases more for shroud extension configurations than SVD. This indicates the order of static pressure rise at this flow coefficient. The SE 40 showed higher pressure rise, whereas the BC 20 showed lowest pressure rise. The

decrease in velocity is gradual for BC 05, BC 10 and BC 20 up to radius ratio 1.25. Thereafter, the velocity reduces up to R = 1.4, but still less compared to SVD. Amount of decrease in absolute velocity depends upon the effectiveness of the diffusion process.

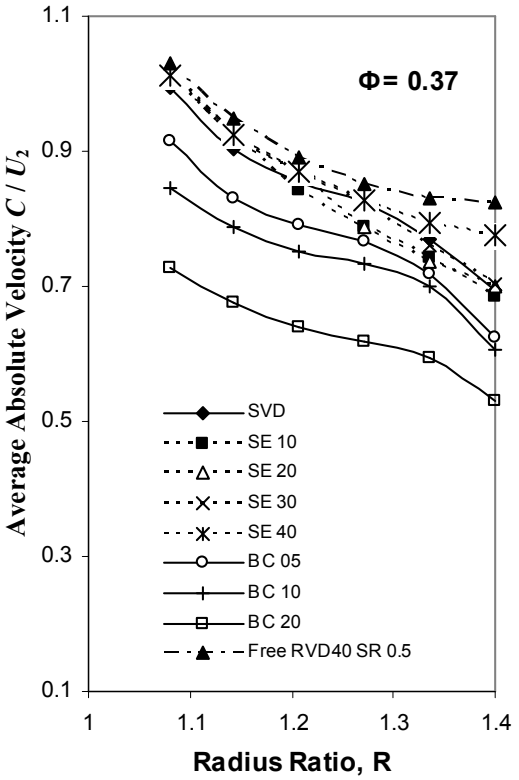

Fig. 7. Radial Distribution of Mass Averaged Non-Dimensional Absolute Velocity for SVD, Shroud Extension and Blade Cutback.

3.5. Mass averaged flow angle

Mass averaged flow angle against radius (Fig. 8) indicates that in SVD, flow angle increases within the vaneless passage region up to R=1.3 and then decreases nearly equivalent to that at the inlet, as the flow exits the diffuser. The similar pattern is observed for the blade cutback but with a higher flow angle, which is due to the variation made in the blade tip geometry. As the blade is cut, the blade angle decreases and for the same volume flow rate and peripheral velocity, the flow angle leaving the impeller increases. For shroud extension, the flow angle does not change significantly in the radial direction. The flow angle remains constant as the radius increases for SE 30 and SE 40. The flow angles for shroud extension are less compared to SVD and blade cutback.

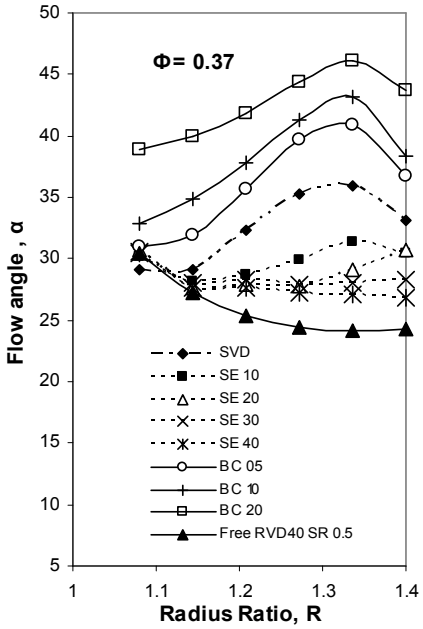

Fig. 8. Radial Distribution of Mass Averaged Flow Angle for SVD, Shroud Extension and Blade Cutback.

3.6. Contours of Static and Stagnation Pressures

Static pressure in general increases with radius due to flow diffusion (Fig. 9). As the disks rotate, the fluid particles adhering to the periphery of the disk rotate with the same angular velocity. The angular velocity of the fluid particle will decrease with the distance from the wall. The increased kinetic energy of the fluid results in static pressure gain as the flow moves to higher radius. Hence, the static pressure is slightly higher near the walls (x/b =0.1 and x/b = 0.9) compared to the mid axial location (x/b = 0.5) where the fluid particles are unlikely to gain the rotational velocity from the disks. The flow is not fully diffused at the exit of the diffuser, though the variation in the axial direction is more uniform compared to the impeller exit plane.

The stagnation pressure is fairly uniform at x/b =0.5 compared to other two axial locations (Fig. 10). The flow mixes out as it reaches the exit of the diffuser for x/b = 0.5. At x/b = 0.9, the flow is non-uniform even at the exit. The wake and jet flow with high and low pressure zones are visible at the exit of the impeller. The stagnation pressure decreases as the radius ratio is increased due to frictional and turbulent mixing losses. Total pressure is high near hub and shroud walls compared to x/b = 0.5.

The main pressure losses of low specific speed stages are due to windage (disk friction and recirculation) and skin friction. On high specific stages, they are mostly due to curvature and diffusion in the impeller. The low tangential angles

of the flow leaving the low specific speed impellers such as the present impeller produce long logarithmic path lengths. This, combined with the low hydraulic radius of the corresponding vaneless diffusers, produce high skin friction losses.

One method of reducing the shear losses on the vaneless diffuser sidewalls, with probable improved efficiency and flow range of low to medium specific speed stages, is the use of a "rotating diffuser".

If the vaneless diffuser sidewalls are stationary, the dynamic head and the logarithmic path length of the flow casing the shear losses are functions of the magnitude and direction of the absolute velocity leaving the impeller. On the other hand, if the vaneless diffuser sidewalls are rotating, the dynamic head and the path length of the flow causing the shear losses are a function of the magnitude and direction of the relative velocity in the diffuser, which is much smaller and more radial than the absolute velocity. Thus the boundary layer growth within the rotating diffuser is smaller than in the corresponding stationary diffuser, and the compressor performance improves.

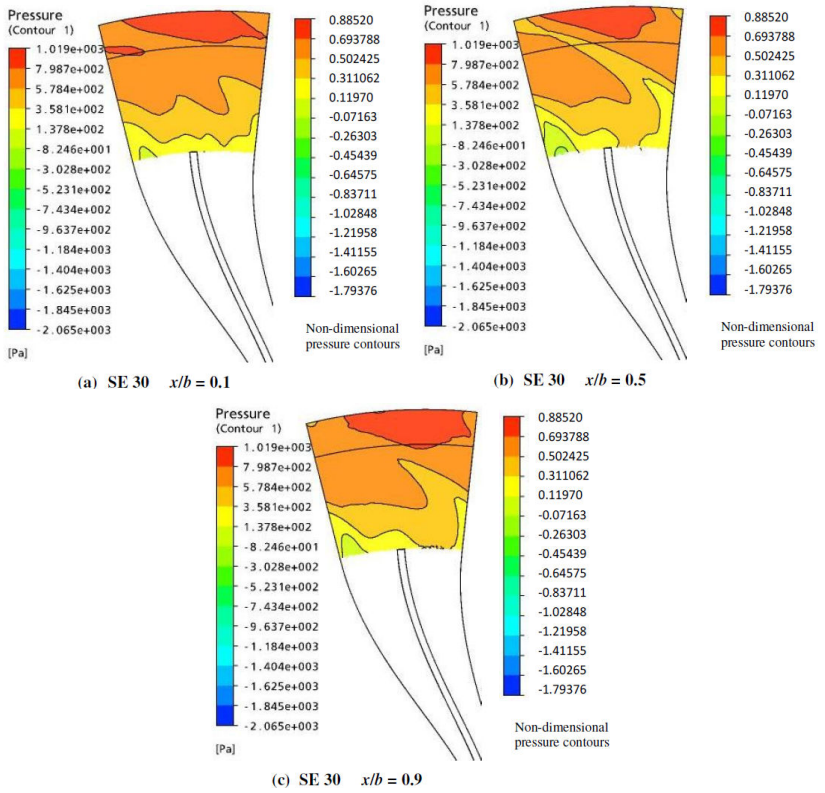

Fig. 9. Contours of Static Pressure Distribution on the Axial Plane at x/b = 0.1, 0.5, 0.9 and Φ = 0.37 for SE 30

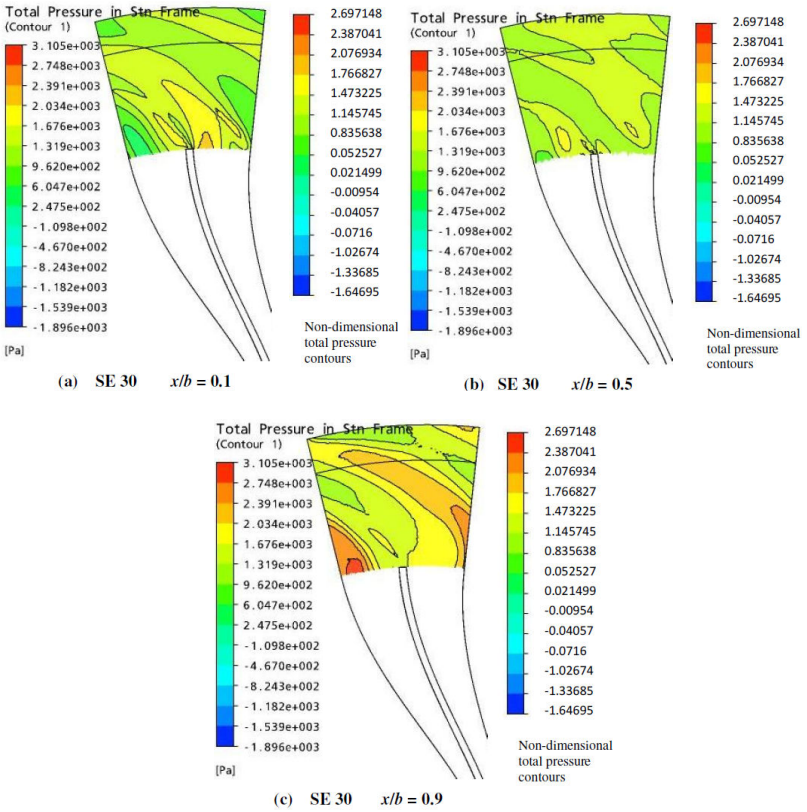

Fig. 10. Contours of Total Pressure Distribution on the Axial Plane at x/b = 0.1, 0.5, 0.9 and Φ = 0.37 for SE 30.

In addition, the rotating diffuser walls impart tangential momentum to the fluid which increases the tangential velocity due to viscous action. Combining the above two effects, it is possible for the total pressure to increase in the diffuser.

4. Conclusions

The performance characteristics of various blade cutback configurations are less in terms of efficiency, energy coefficient, specific work, as well as static pressure rise. Therefore, blade cutback concepts are not suitable to attain the desired objective with radial bladed impeller ($\beta_2 = 90^0$). This is due to alterations made in blade tip geometry by blade cutback concepts, which have a greater effect on the velocities of the through flow.

The objective of obtaining higher static pressure rise with reduced losses over SVD is achieved by SE 30, followed by SE 20. This explains that the rate of diffusion is higher in shroud extension compared to SVD. Shorter flow path length and higher relative flow angle cause lower frictional losses in shroud extension configurations compared to SVD. The efficiency, energy coefficient and the specific work of SE 30 is higher than SVD.

References

1. Rodgers, C. (1976). Design and test of an experimental rotating diffuser centrifugal compressor test rig. *SAE International*, *Paper No. 760927*, DOI: 10.4271/.
2. Erwin, J.R.; and Vitale, N.G. (2008). Radial outflow compressor design (Gas turbine engineering). Wexford College Press.
3. Sapiro, L. (1983). Effect of impeller-extended shrouds on centrifugal compressor performance as a function of specific speed. *ASME Journal of Engineering for Power*, 105(3), 457-465.
4. Govardhan, M.; Murthy, B.S.N.; and Gopalakrishnan, G. (1978). A preliminary report on rotating vaneless diffuser for a centrifugal impeller. *Proceedings of the First International Conference on Centrifugal Compressor Technology,* D4-1 – D4-5, IIT Madras, India.
5. Linder, P. (1983). Aerodynamic tests on centrifugal process compressors – influence of diffuser diameter ratio, axial stage pitch and impeller cutback. *ASME Journal of Engineering for Power*, 105, 910-919.
6. Yves, R.; and Christian, F. (1989). Re-evaluation of researches on the free rotating vaneless diffuser. *ASME International Gas Turbine and Aero-engine Congress and Exposition*, Toronto, Canada.
7. Aboujaib, M.; Bayeul, M.L.; and Annie, C. (1998). Computational fluid dynamics '98. *Proceedings of the 4th European Computational Fluid Dynamics Conference,* Athens, Greece, 1, 279-284.